2018

Spin-polarized electron transmission through chiral halocamphor molecules

J. M. Dreiling

F. W. Lewis

T. J. Gay

Journal of Physics B: Atomic, Molecular and Optical Physics

LETTER • **OPEN ACCESS**

Spin-polarized electron transmission through chiral halocamphor molecules

OPEN ACCESS
IOP Publishing

Letters
Journal of Physics B: Atomic, Molecular and Optical Physics

J. Phys. B: At. Mol. Opt. Phys. **51** (2018) 21LT01 (6pp) https://doi.org/10.1088/1361-6455/aae1bd

Letter

Spin-polarized electron transmission through chiral halocamphor molecules

J M Dreiling[1,3], F W Lewis[2] and T J Gay[1]

[1] Jorgensen Hall, University of Nebraska, Lincoln, NE 68588-0299, United States of America
[2] Department of Applied Sciences, Faculty of Health and Life Sciences, Northumbria University, Newcastle upon Tyne, NE1 8ST, United Kingdom

E-mail: jmdreiling2@gmail.com

Received 3 September 2018
Accepted for publication 17 September 2018
Published 15 October 2018

Abstract

We have measured electron-circularly-dichroic asymmetries when longitudinally-polarized (chiral) electrons are scattered quasi-elastically by chiral halocamphor molecules: 3-bromocamphor ($C_{10}H_{15}BrO$), 3-iodocamphor ($C_{10}H_{15}IO$), and 10-iodocamphor. The proposed dynamic origins of these asymmetries are considered in terms of three classical models related to Mott scattering, target electron helicity density, and spin-other-orbit interactions. The asymmetries observed for 3-bromocamphor and 3-iodocamphor scale roughly as Z^2, where Z is the nuclear charge of the heaviest atom in the target molecule, but the scaling is violated by 10-iodocamphor, which has a smaller asymmetry than that for 3-iodocamphor. This is in contrast to the asymmetries in the collision channel associated with dissociative electron attachment, in which 10-iodocamphor has a much larger asymmetry. All of the available electron-circularly-dichroic data taken to date are considered in an effort to systematically address the dynamical cause of the observed chiral asymmetries.

Keywords: electron scattering, spin dependence of cross sections, chirality, electron circular dichroism

(Some figures may appear in colour only in the online journal)

When longitudinally-polarized electrons scatter from gas-phase chiral molecules, the scattering cross section for a given collision channel will generally depend on the chirality of both collision partners. This was first demonstrated more than two decades ago with targets of $Yb(hfc)_3$ for the quasi-total scattering cross section measured by the beam-attenuation, or 'transmission' method [1]. These studies were subsequently extended to a variety of other molecules; all non-zero chiral effects measured to date have involved molecules containing at least one atom with a relatively high atomic number ($\geqslant$35) [2, 3]. Recently, similar 'electron dichroic' effects were seen in electron-induced dissociative reactions ('dissociative electron attachment' or DEA) in 3-bromocamphor and 3- and 10-iodocamphor [4, 5]. In all these experiments, the chiral sensitivity of a given reaction channel is characterized by an asymmetry parameter a:

$$a_{+(-)} = \left[\frac{(I_\uparrow - I_\downarrow)}{(I_\uparrow + I_\downarrow)}\right]_{+(-)}, \quad (1)$$

where I corresponds to the detected current for a given scattering channel with spin-forward ($\uparrow$) or spin-backward ($\downarrow$) incident electrons. The '+' and '−' subscripts refer to the handedness of the chiral target. Experiments with gas-phase

[3] Current address: Honeywell, Broomfield, CO 80021, United States of America.

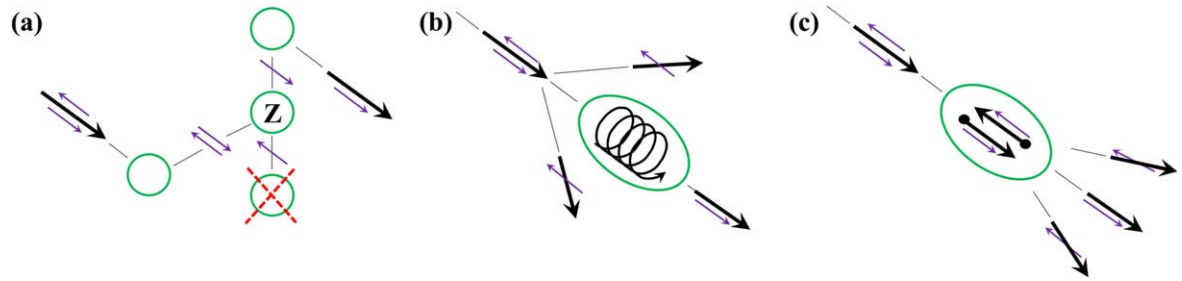

Figure 1. Schematic diagrams of collisional mechanisms in transmission experiments leading to chiral asymmetries showing (a) Mott scattering, (b) spin-other-orbit coupling, and (c) helicity density (see text). Figure adapted from reference [5].

chiral targets have an advantage over those with fixed targets in that any measured non-zero value of a constitutes a clean signature of the effect of target chirality in the scattering process; fixed-target experiments can exhibit similar effects due solely to chiral collision geometry. The disadvantage of random target orientation is that the values of a are generally quite small, rarely exceeding 2×10^{-4}. An interesting exception to this is the case of 3-iodocamphor in the DEA channel, for which a is about an order of magnitude larger [5].

While the chiral symmetry of these experiments permits a to be non-zero, it provides no clues as to the dynamical mechanisms that might produce such electron-dichroic effects. The studies mentioned above have generally been designed to answer this question by varying either the molecular target's Z—the atomic number of the molecule's heaviest atom—or the target's stereochemical structure, or both. These efforts have largely failed to provide unambiguous evidence of a specific, generally applicable mechanism of chiral selectivity [5–7]. Moreover, no broad theoretical effort has yet been mounted to shed light on this problem. The experiments reported here, measurements of transmission asymmetries with 3-bromocamphor and 3- and 10-iodocamphor, provide new information relevant to some aspects of chirally-sensitive scattering, but they also fail to identify a single, overarching dynamical scattering model that explains the asymmetries we observe. Nonetheless, they do permit us to make the most comprehensive assessment to date of chiral collision dynamics in electron–molecular collisions.

Three qualitatively different mechanisms have been proposed in the literature to account for electron circular dichroism in both transmission and in DEA. We refer to them as 'Mott/plural scattering', 'spin-other-orbit coupling', and 'helicity-density' dynamics (see figure 1). They are discussed here specifically for transmission measurements in terms of simple classical pictures that explain why one direction of longitudinal electron spin is more likely to be scattered than the other [6–12]. (Similar classical pictures that pertain to DEA have been described elsewhere [5].)

In Mott/plural scattering [9], an incident electron is first Coulombically scattered away from the forward direction by a relatively light atom in the target (figure 1(a)), changing the electron's momentum without significantly affecting its spin. Subsequent large-angle Mott scattering from the high-Z atom in the molecule has a preferential direction that depends on the incident electron's spin. This in turn can result in enhanced scattering back into the forward direction for, e.g., spin-forward electrons. In figure 1(a), the chirality of the molecule is such that the lower atom, which could rescatter the electron with 'backward' spin, is missing on average (illustrated as the crossed-out atom). While such an effect can also occur with an oriented achiral target, it would average to zero over all molecular orientations. Mott asymmetries of the type discussed here scale as Z^2 [13].

Spin-other-orbit interactions (figure 1(b)) occur due to current in the target molecule driven by the Coulombic impulse of an approaching electron [10, 11]. Thinking of a chiral molecule as a conducting helix, it is apparent that such a current will produce both electric and magnetic dipole moments that can act back on the approaching electron. The spin of the incident electron will interact with the magnetic moment produced by the induced orbital angular momentum of the target electrons (the 'spin-other-orbit' coupling), leading to differences in scattering that depend on the electron's helicity. Interference between such induced electric and magnetic dipoles is responsible for optical activity in chiral samples [12]. This effect does not require the presence of a heavy atom in the molecule, but instead relies primarily on the molecular polarizability, which is more closely related to the molecular mass than Z. Thus if spin-other-orbit coupling is the primary mechanism for electron dichroic effects, one might expect there to be a correlation between a and the molecule's optical rotatory power (ORP), a quantification of a molecule's optical activity determined by measuring the angle of rotation that the electric field vector of linearly-polarized light experiences while passing through a chiral solution.

Finally, the spin–orbit interaction between a high-Z nucleus and the electrons in a chiral molecule will generally lead to a non-zero expectation value of the 'helicity density' operator, $\langle \boldsymbol{\sigma} \cdot \mathbf{v} \rangle$, for the electrons inside the molecule [6, 14, 15]. Here, $\boldsymbol{\sigma}$ and $\mathbf{v}$ are the electron spin and velocity vectors, respectively. This is true even though $\langle \boldsymbol{\sigma} \rangle = 0$ and $\langle \mathbf{v} \rangle = 0$; the chirality of the target's stereochemistry manifests itself in the chirality of the target electrons. If a target electron is headed in a particular direction within the chiral molecule, its spin will have a non-zero average projection along that direction as well. Helicity density can affect electron scattering if a dynamical difference exists between the scattering of an incident electron by target electrons that have velocity components of opposite sign along the beam direction (figure 1(c)). Assume, for example, that only electrons

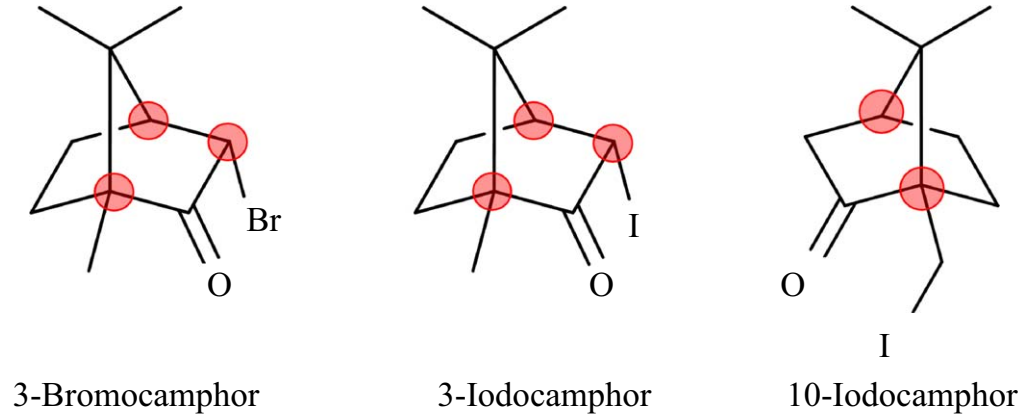

Figure 2. Chiral camphor-derivative molecules studied in this experiment. The (+)-enantiomers are shown, and chiral centers are indicated with red circles.

with velocity components anti-parallel to the beam direction act to scatter incoming electrons to an appreciable angle, and that the target handedness is such that these electrons tend to have a component of spin parallel (as opposed to anti-parallel) to that direction. There would thus be a different cross section for the scattering of one incident electron helicity over the other because of the differences in the singlet versus the triplet cross sections. Since the helicity density is produced primarily by the spin–orbit interaction of target electrons with the heaviest target nucleus, these effects should also scale as Z^2 [14].

In the transmission experiments reported here, the targets are variants of camphor in which one hydrogen atom is replaced with either a bromine ($Z = 35$) or iodine ($Z = 53$) atom. These molecules were chosen because they have a reasonably high vapor pressure, they contain a high-Z atom, and we were able to either purchase or synthesize them in both enantiomeric forms. In the case of iodocamphor (see figure 2), the iodine was either attached at a position immediately adjacent to one of the molecule's chiral centers (3-iodocamphor, which we refer to as '3I'), giving a structure equivalent to 3-bromocamphor ('3Br'), or at a position separated from another chiral center by two serial bond lengths (10-iodocamphor, '10I').

In our previous measurements of DEA (as opposed to transmission) asymmetries with 3Br and 3I [4, 5], a scaled almost perfectly with Z^2. We were thus surprised when 10I, which we would have expected in a Mott/plural scattering picture to have significantly lower a, exhibited instead the largest value of a observed to date ($>10^{-3}$). Our subsequent calculations of helicity density for 10I indicated much-reduced values compared with those for 3I. There was also no obvious correlation in our DEA data with the ORP of these compounds, apparently ruling out a spin-other-orbit mechanism. Thus, the chiral interaction mechanism(s) responsible for asymmetries in DEA could not be identified. The measurements of chiral asymmetry in transmission reported here were undertaken to clarify the role that the three mechanisms might play in a different interaction channel.

The apparatus used for these measurements has been discussed elsewhere [4, 16], so only the most relevant details will be included here. Longitudinally-spin-polarized electrons were photoemitted from a GaAs photocathode [17], with the spin direction determined by the circular polarization of the incident light. The energy width of the electron beam was ~0.5 eV, and its polarization was typically ~30% as measured by an optical polarimeter [18]. To reduce instrumental asymmetries, we made use of the feedback system described in reference [19] which combined a spatial filter and quarter-wave plate in the optical setup used for photoemission. The incident electron beam entered the target cell (depicted in figure 3) with the collision energy determined by the voltage applied to the inner target cell. The target cell was kept at ~100 °C to prevent target molecules from condensing on the electron-optic elements. Inside the target cell, the electron beam was scattered by a chirally-pure molecular target vapor through various interaction channels including, but not limited to, DEA, quasi-elastic scattering, and vibrational excitation. The voltages applied to the retarding meshes following the target cell (elements 6 and 7 in figure 3) were set to discriminate against electrons that had lost energy in collisions with target molecules, and therefore only the quasi-elastically-scattered electrons were allowed to pass out of the target cell and be collected in the Faraday cup.

To perform an asymmetry measurement, molecules of a given handedness were admitted to the target cell until the transmitted electron beam current was reduced to ~30% of its unattenuated value. The 'transmission' asymmetry (equation (1)) for these experiments was determined with I being the Faraday cup current (designated as I_t in figure 3). A final asymmetry value, A, was calculated using

$$A = a_- - a_+ = \left[\frac{(I_\uparrow - I_\downarrow)}{(I_\uparrow + I_\downarrow)}\right]_- - \left[\frac{(I_\uparrow - I_\downarrow)}{(I_\uparrow + I_\downarrow)}\right]_+. \qquad (2)$$

At each energy, A was measured ~10 times, and an average was found after applying Chauvenet's criteria [20] to the data. Statistical uncertainties are given by the standard deviation of the sample mean. By collecting data with two different settings of the quarter-wave plate that circularly polarized the light used to photoemit the electron beam [19], an overall phase shift was introduced into the experiment, and the sign

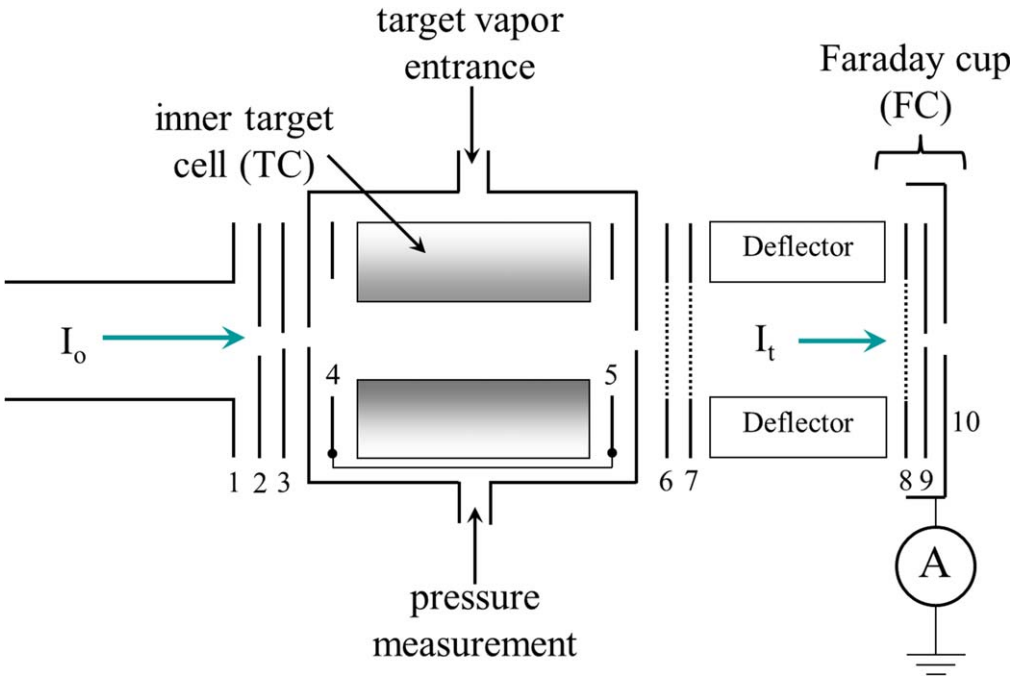

Figure 3. Schematic of the target elements, including the incident (I_o) and transmitted (I_t) electron beams, the target cell structure, and the Faraday cup assembly (elements 8–10) used to measure the transmitted beam. Other electrostatic lens elements (1, 2, 4, 5), retarding-field meshes (6, 7), and a beam-defining aperture (3) are indicated as well. Reprinted figure with permission from [4], Copyright (2014) by the American Physical Society.

of the measured asymmetry was therefore reversed. The systematic uncertainty was taken to be the absolute value of the sum of the measurements obtained with opposite quarter-wave plate settings. When data was taken with only one of the settings of the quarter-wave plate (as is the case for most of the 3Br data), only the statistical uncertainty is reported. When data was collected at both quarter-wave plate settings, the uncertainty was obtained by combining the statistical and systematic uncertainties in quadrature.

Our transmission data for 3Br, 3I, and 10I are shown in figure 4. (In the following discussion, all values of A will be given in units of 10^{-4}.) The differences between these data and those for DEA with the same targets [5] are striking. The values of A for 3Br in transmission have a maximum magnitude of ∼0.7; those in DEA approach 4. In contrast with our DEA experiments, the A-values for the 10I targets in transmission are generally smaller than those for 3I. We assign the largest value for 3I to be 1.1(6) by taking the error-weighted average of the magnitude of the data at 1.0 and 1.4 eV, whereas for 10I, we measure values of A that are consistent with zero. In contrast, the maximum A values in DEA for 3I and 10I are about 8 and 16, respectively!

The current status of all electron-circular-dichroic measurements that have been made to date in both transmission and DEA [1–5, 8, 16] are summarized in figures 5–7. In order to assess the validity of the three mechanisms discussed above, we have plotted A values both as a function of Z^2 and the ORP of the target. If the chiral scattering mechanism is best described by Mott/plural scattering or a helicity density picture, A should scale linearly with Z^2. Given the close connection between the spin-other-orbit picture of electron scattering and the magnetic/electric dipole interference responsible for optical activity, a clear correlation between A and the ORP would support a spin-other-orbit picture. The ORP values for all compounds were obtained from the Sigma-Aldrich website [21], with the exception of 3I and 10I, which were determined from references [22] and [23], respectively. All ORPs were measured using sodium D light ($\lambda = 589$ nm).

Figures 5–7 categorize data for three classes of molecular targets: camphor and some of its halocamphor and dihalocamphor derivatives, halomethylbutanes, and a class of rare-earth (lanthanide) NMR shift reagents in which three camphor-like-ligands (3-(heptafluorpropylhydroxymethylene) camphorate (hfc)) surround the rare-earth atom. The Münster group [1–3] has taken all of the halomethylbutane, the rare-earth hfc, and the dibromocamphor data, exclusively in transmission. Both the Münster group and our group have taken transmission data for camphor [1, 8] and 3Br [2, 16], with the results being in good agreement. Our group has taken the DEA halocamphor data [4, 5] and the transmission data for 3I and 10I presented here. It should be emphasized that the experimental parameters for our transmission studies were different from those of the Münster group. Specifically, they used an electron beam of energy width ∼0.3 eV and polarization of ∼40%, and the electron beam was attenuated by ∼90% due to target scattering. To make a valid comparison between our data and theirs in figures 5(a) and (b), we scaled their bromocamphor and dibromocampor data to match our experimental conditions as discussed in reference [16]. The Münster halomethylbutane and rare-earth hfc data (figures 6 and 7) are taken directly from the values they reported

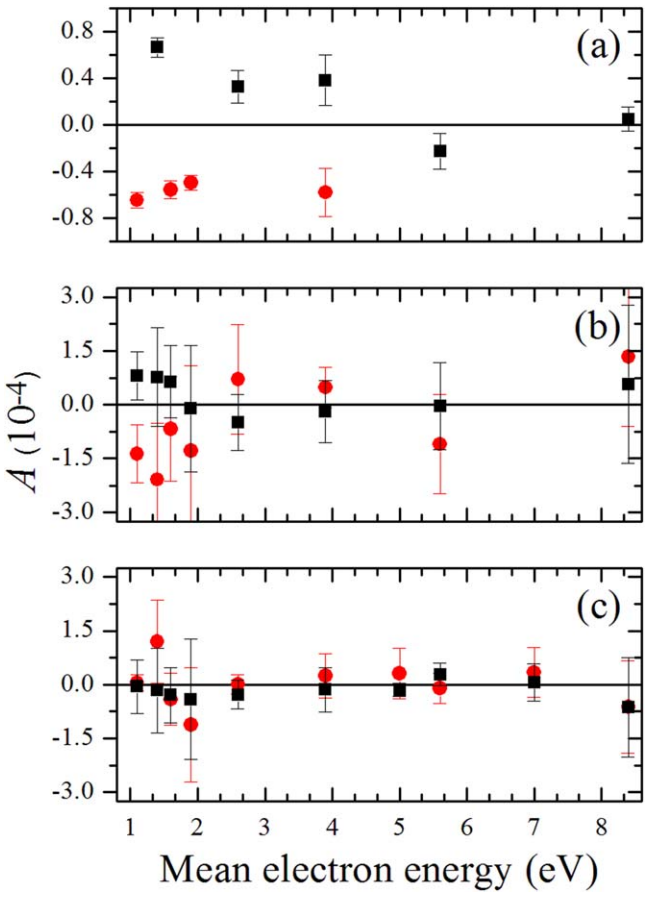

Figure 4. Measured transmission asymmetries, A, as a function of mean electron energy for each halocamphor compound investigated in this study: (a) 3-bromocamphor (3Br), (b) 3-iodocamphor (3I), and (c) 10-iodocamphor (10I). Squares (black) and circles (red) represent opposite settings of the final quarter-wave plate, which should give asymmetry measurements of opposite sign. When asymmetry data was collected at both quarter-wave plate settings, the uncertainty was calculated by finding the quadrature sum of the statistical and systematic uncertainties (see text). For data collected at only one quarter-wave plate setting, the reported uncertainty is just the statistical uncertainty.

without any energy convolution or adjustment for incident electron polarization or electron beam attenuation factors.

The data used to create figures 5–7 are the largest reported absolute values of A for a given collision channel and target for incident electron energies >1 eV. In some compounds, A increases rapidly at the lowest energies investigated. However, as discussed in reference [2] and based upon our own experience, these lowest-energy data are likely contaminated by instrumental effects, and they are therefore not included. This way of presenting the data ignores an important aspect of the electron–molecule chiral interaction: its energy dependence and the probable importance of negative ion resonances. By focusing on the largest value of A for a given target and reaction channel, though, we are presumably selecting the case of optimal collision conditions for chiral interactions and can focus on the zeroth-order problem—possible correlations of A with Z^2 and/or the target's ORP.

The following conclusions may be drawn from the data.

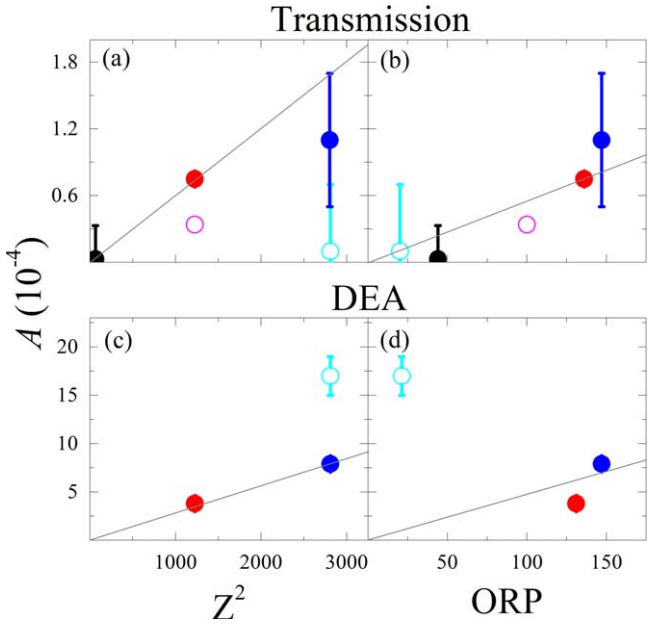

Figure 5. Electron circular dichroism asymmetries, A, with camphor-derivative targets for both quasi-elastic scattering in transmission ((a), (b)) and dissociative electron attachment (DEA; (c), (d)). The data are plotted as a function of the optical rotatory power (ORP) and Z^2, where Z is the highest nuclear charge in the molecule. Open circles denote either 10-iodocamphor (light blue) or 3,9-dibromocamphor (magenta), and solid circles correspond to camphor (black), 3-bromocamphor (red), and 3-iodocamphor (blue). The solid lines are linear fits to the data forced through zero.

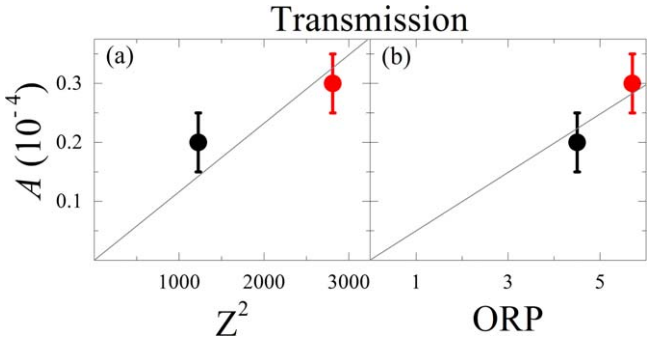

Figure 6. Values of A for the halomethylbutane targets of bromomethylbutane (black) and iodomethylbutane (red).

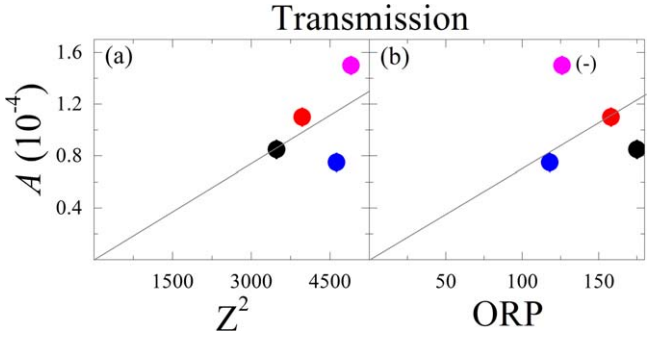

Figure 7. Values of A for the rare-earth targets of $Pr(hfc)_3$ (black), $Eu(hfc)_3$ (red), $Er(hfc)_3$ (blue), and $Yb(hfc)_3$ (magenta). The (-) indicates that the sign of the ORP for the $Yb(hfc)_3$ target is opposite that of the others.

Camphor-derivatives (*figure* 5). We consider first only the molecules in which the high-Z atom is varied exclusively in the 3-position: camphor, 3Br, and 3I. Both the transmission (figure 5(a)) and DEA (figure 5(c)) data scale linearly with Z^2, but this does not allow us to distinguish between the helicity density and Mott/plural scattering mechanisms. Much is learned, however, by adding the 10-iodocamphor and the 3,9-dibromocamphor results. The 10I DEA data (figure 5(c)) cannot be explained in either a simple Mott scattering picture or by a helicity density calculation [5]. However, in transmission, the helicity density model does account for the reduction of A for both dibromocamphor [6] and 10I [5]. We thus argue that while the transmission data is consistent with Mott/plural scattering, it has more comprehensive, quantitative theoretical support from helicity density calculations [5]. Unfortunately, this view is blurred by the fact that all of the transmission data exhibit a smooth, monotonic (albeit non-linear) increase of A with ORP (figure 5(b)). The ORP scaling is non-existent for DEA (figure 5(d)).

Halomethylbutane derivatives (*figure* 6). The transmission data scale linearly with both Z^2 and the ORP, so no conclusions can be drawn.

Rare-earth complexes (*figure* 7). Unlike the halomethylbutanes, where A correlates nominally with both ORP and Z^2, there is no obvious scaling of any kind with the rare-earth hfcs. We note that while the ORP values are positive for three of the targets, the largest A occurs for Yb(hfc), which actually has a negative ORP.

The camphor-family transmission data, shown in figures 5(a) and (b), have provided the most complete picture to date of how a chiral stereochemical system scatters polarized electrons. Like the DEA 3Br and 3I data, the transmission data scale well with Z^2, but with transmission, the 10I and dibromocamphor data departures from this simple scaling can be explained semi-quantitatively by helicity density calculations [5, 6] and, in a more hand-waving way, by a Mott scattering picture. This would seem to give a first, incremental understanding of the electron-chiral molecule scattering problem, were it not for the fact that the transmission A-values for the entire camphor family lie on a fairly smooth, monotonically-increasing curve that is a function of the ORP of the target. Overall, these emergent patterns of functional dependence still do not allow us to identify unambiguously a dynamical scattering model for these targets. It is at least clear that DEA and quasi-elastic total scattering rely differently upon the (crudely-characterized) classical mechanisms we have identified here.

It would be interesting to revisit the rare-earth hfc targets, which are 'propeller' molecules, having the high-Z rare-earth atom at the hub of the three camphorate-ligand (hfc) 'blades.' The Münster data were taken with targets in which all the blades had the same camphor-like chirality, but which were racemic mixtures of left- and right-handed blade configurations. Thus, the heavy atom was not at a chiral center of the molecule. New experiments with targets having chirally-pure blade arrangements might yield a correlation of A with either Z^2 or ORP. More generally, the future of these studies must surely include a more robust theory effort.

Acknowledgments

The authors would like to thank P D Burrow for his substantial assistance throughout this project. This work was funded by the US National Science Foundation, Grant Nos. PHY-1206067 and PHY-1505794. We also thank Northumbria University for awarding an Anniversary Research Fellowship to FWL.

ORCID iDs

J M Dreiling https://orcid.org/0000-0001-9226-203X
F W Lewis https://orcid.org/0000-0003-3176-8162
T J Gay https://orcid.org/0000-0001-9208-1570

References

[1] Mayer S and Kessler J 1995 *Phys. Rev. Lett.* **74** 4803
[2] Mayer S, Nolting C and Kessler J 1996 *J. Phys. B: At. Mol. Opt. Phys.* **29** 3497
[3] Nolting C, Mayer S and Kessler J 1997 *J. Phys. B: At. Mol. Opt. Phys.* **30** 5491
[4] Dreiling J M and Gay T J 2014 *Phys. Rev. Lett.* **113** 118103
[5] Dreiling J M, Lewis F W, Mills J D and Gay T J 2016 *Phys. Rev. Lett.* **116** 093201
[6] Scheer A M, Gallup G A and Gay T J 2006 *J. Phys. B: At. Mol. Opt. Phys.* **39** 2169
[7] Gay T J 2009 *Adv. At. Mol. Phys.* **57** 157
[8] Trantham K W, Johnston M E and Gay T J 1995 *J. Phys. B: At. Mol. Opt. Phys.* **28** 1543
[9] Kessler J 1982 *J. Phys. B: At. Mol. Phys.* **15** 101
[10] Walker D W 1982 *J. Phys. B: At. Mol. Phys.* **15** 289
[11] Gallup G A 1994 *Electron Collisions with Molecules, Clusters, and Surfaces* ed H Ehrhardt and L A Morgan (New York: Plenum) pp 163–70
[12] Condon E U 1937 *Rev. Mod. Phys.* **9** 444
[13] Mott N F and Massey H S W 1965 *The Theory of Atomic Collisions* 3rd edn (New York: Oxford) p 235
[14] Rich A, Van House J and Hegstrom R A 1982 *Phys. Rev. Lett.* **48** 1341
[15] Gay T J, Johnston M E, Trantham K W and Gallup G A 1996 *Selected Topics in Electron Physics* ed D M Campbell and H Kleinpoppen (New York: Plenum) pp 159–70
[16] Dreiling J M and Gay T J 2015 *J. Phys.: Conf. Ser.* **635** 012015
[17] Pierce D T, Celotta R J, Wang G-C, Unertl W N, Galejs A, Kuyatt C E and Mielczarek S R 1980 *Rev. Sci. Instrum.* **51** 478
[18] Gay T J, Furst J E, Trantham K W and Wijayaratna W M K P 1996 *Phys. Rev.* A **53** 1623
[19] Dreiling J M, Burtwistle S M and Gay T J 2015 *Appl. Opt.* **54** 763
[20] Bevington P R and Robinson D K 1992 *Data Reduction and Error Analysis for the Physical Sciences* (New York: McGraw-Hill) p 58
[21] http://sigmaaldrich.com/united-states.html
[22] Mathieu J P and Perrichet J 1935 *C. R. Hebd. Seances Acad. Sci.* **200** 1583
[23] Lewis F W, Egron G and Grayson D H 2009 *Tetrahedron: Asymmetry* **20** 1531